DESIGN AND ANALYSIS OF SLAT SYSTEMS IN TRANSONIC FLOW

B. Arlinger, Saab-Scania, Sweden

W. Schmidt, Dornier, West Germany

Abstract

A numerical method for the analysis of two-dimensional transonic flow around two-element airfoil configurations has been extended to treat mixed analysis and design problems. By prescribing the pressure distribution along a part of one airfoil a new contour shape results. The method also works for thick trailing edges. Results are presented which show the redesign of slat lower surfaces.

The boundary layer is accounted for in a couple of calculations where the displacement thickness have been added to the original shapes.

A systematic analysis series is also presented of the effect of various geometric parameters on the pressure distribution about a slat-airfoil configuration.

1. Introduction

When designing modern aircraft often high requirements on maneuvering performance at high subsonic speeds has to be met together with strong requirements on the cruise performance in terms of drag or speed. An effective way of meeting these different demands is the implementation of high lift devices in the form of leading edge slats and trailing edge flaps. For the proper design of these devices in low speed flow, efficient calculation methods and extensive experimental material exist.

However, in the transonic speed regime the wind tunnel results on airfoils with slats and/or flaps are quite few, and the question of optimal shapes and deflections for the devices is still open. Since about two years calculation methods for the analysis of transonic flow over two-element airfoil systems exist[1-3]. They are based on the full potential equation, which is solved in a calculation plane obtained by conformal mapping of the two airfoils.

The technique applied in these methods to generate new coordinates by conformal mapping has proven its effectiveness in many applications[4,5], and so has the numerical solution technique for mixed subsonic-supersonic flow fields originally introduced by Murman[6] and further developed by Jameson[7].

The two-element methods are very valuable tools for the designer, but extensions and improvements can still be made.

In the present work the calculation method presented in Ref. 2 is extended to treat also the mixed direct and inverse problem. The pressure distribution can be prescribed along a suitable part of one airfoil and the corresponding shape is calculated.

Also presented is an extension of the mapping used in Ref. 2 so that airfoils with thick trailing edges can be treated. This is of interest in design calculations and especially when viscous effects are taken into account by adding the displacement thickness to the contour.

A short description is given of the acceleration technique based on extrapolation that is used in the calculations to improve the convergence rate of the successive line overrelaxation process.

The technique used when accounting for the boundary layer effects is presented together with a few examples. The viscous effects are in many cases quite large due to separated boundary layers, for instance on slat lower surfaces. An accurate modelling of such cases still belongs to the future.

However, a well designed slat configuration for transonic maneuvering should have no extensive separated regions to avoid large drag increments. The effect of various parameters such as slat location, camber, slat geometry, Mach number, etc has to be investigated systematically to get configurations with good performance. The effect of some of these parameters is shown in the present work by demonstrating their influence on the pressure distributions.

2. The calculation method

Here a short description is given of the basic calculation method before dealing with the new boundary conditions.

For a more detailed presentation of the theory the reader is referred to Ref. 2.

Coordinate system

The coordinate system used for the numerical solution of the potential equation is obtained by conformally mapping the contours in the physical plane to geometrically simple contours in a calculation plane. This way of generating coordinates has proven its effectiveness in many applications. It has the advantage of yielding simple formulations of the boundary conditions and also simple equations, because orthogonality is preserved in the mapping. A disadvantage with conformal mapping can be a rather complex programming work, as in the present case. However, once the program is made it works automatically for all shapes, and the computing times for the mapping are always small compared to the times used for the relaxation solution of the flow equations.

Fig. 1 illustrates the mapping used in the present method. The whole flow field around an arbitrary two-element configuration is mapped conformally to the annular region between two concentric circles (with radius r_s and 1 respectively). In this calculation plane a polar coordinate system is used where the radial and circumferential variables can

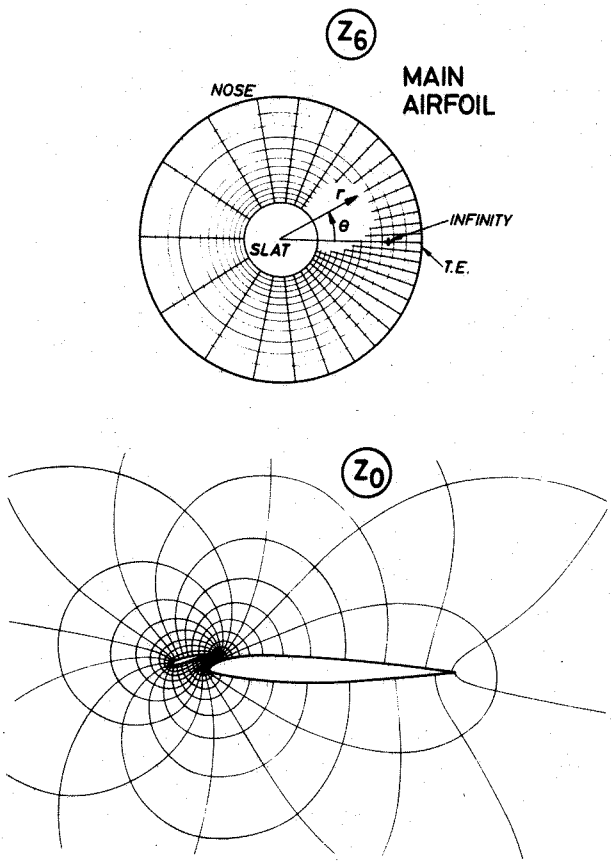

Fig. 1 Corresponding grids in the computational and physical planes

be stretched independently to improve the mesh size distribution in the physical plane. The relations used between the stretched (r', θ') and the original (r, θ) polar coordinates are

$$r' = (1+k) \ln \frac{r+k}{1+k} \qquad (1)$$

$$\theta = \theta' + c_1 \sin \theta' + c_2 \sin 2\theta' \qquad (2)$$

where k, c_1 and c_2 are constants.

The infinity is mapped to a point in the calculation plane located on the real axis. The constant k in Eq.(1) is adjusted so that a mesh point is always located in the infinity point.

The mapping of thick trailing edges

When simulating viscous effects one way is to add the boundary layer displacement thickness to the original contour, thereby getting equivalent airfoil shapes with thick trailing edges.

Mainly for this reason the mapping presented (2) has been extended so that if one or both of the trailing edges have a finite thickness a first mapping step is applied which maps the two contours to a similar configuration, but with sharp trailing edges. The transformation is

$$z_0 = z_1 + \frac{i}{2\pi}\Delta z_{0t1} \ln(z_1 - z_{1s1}) + \frac{i}{2\pi}\Delta z_{0t2} \ln(z_1 - z_{1s2}) \qquad (3)$$

where z_0 is the physical complex plane and z_1 is the mapped plane. The trailing edge thickness vectors and the locations of the logarithmic singularities are illustrated in Fig. 2.

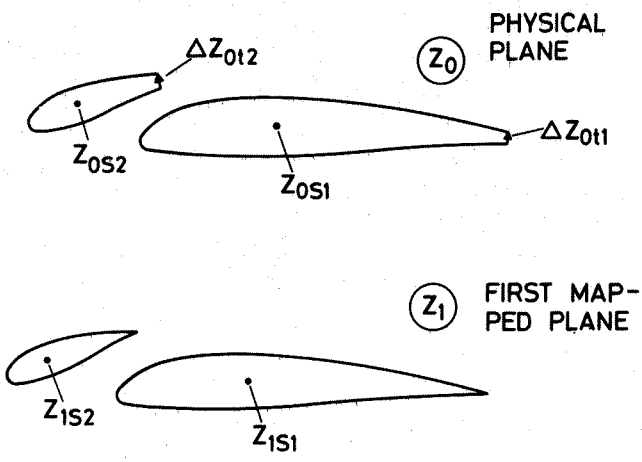

Fig. 2 Notations for the initial mapping step

Because the z_0-coordinates are given, the corresponding z_1-coordinates are calculated from Eq. (3) iteratively.

The physical meaning of this technique is that wakes of constant thickness and without any pressure difference across them leave the trailing edges. This could be considered only as a first approximation to the real trailing edge wakes which start with diminishing displacement thickness and which, if curved, sustain pressure differences across them.

Flow analysis

The mass conservation equation expressed in the calculation plane coordinates is

$$(\rho q_1 B r)_r + (\rho q_2 B)_\theta = 0 \qquad (4)$$

where ρ is the density, q_1 and q_2 are the radial and circumferential velocity components respectively, and B is the mapping modulus defined by

$$B = \left| \frac{dz_0}{dz_6} \right| \qquad (5)$$

z_0 is the physical plane and $z_6 = re^{i\theta}$ is the calculation plane.

Assuming isentropic flow relates density and velocity and implies that the potential, ϕ, can be introduced:

$$\rho^{\gamma-1} = a^2 M_\infty^2 = 1 + \frac{\gamma-1}{2} M_\infty^2 \ (1-q_1^2-q_2^2) \qquad (6)$$

$$q_1 = \frac{1}{B}\phi_r \qquad (7)$$

$$q_2 = \frac{1}{Br}\phi_\theta$$

Here a is the local speed of sound and M_∞ the free stream Mach number. All velocities are made dimensionless by the free stream velocity, and the density by its free stream value.

At present Eq. (4) is rewritten and solved in non-conservative form, which normally gives a better convergence rate and less truncation error than the conservative formulation. However, when all the viscous effects can be accurately modelled the conservative formulation should be used.

The developed form of Eq. (4) used in the present method is the potential equation, arrived at by applying Eqs. (6) and (7)

$$D\phi + (q_1^2 + q_2^2)(q_1 B_r + \frac{q_2}{r} B_\theta) = 0 \qquad (8)$$

where D is the differential operator

$$(a^2-q_1^2)\frac{\partial^2}{\partial r^2} - \frac{2q_1q_2}{r}\frac{\partial^2}{\partial r \partial\theta} + \frac{a^2-q_2^2}{r^2}\frac{\partial^2}{\partial\theta^2} +$$

$$+ \frac{a^2+q_2^2}{r}\frac{\partial}{\partial r} \qquad (9)$$

The potential ϕ is unbounded and manyvalued in the calculation plane because the infinity is represented by a point and due to the circulation around each airfoil.

In Ref. 2 is described in detail how a reduced potential, χ, is introduced which is bounded and singlevalued in the whole calculation plane. The final equation used for computing χ can be written

$$D\chi + DF + G = 0 \qquad (10)$$

where $F = \phi - \chi$ is a large analytic expression in the independent variables and the two circulations. G is a function of the velocity components and the mapping modulus.

The Kutta conditions require that the tangential velocity q_2 is bounded at the trailing edges. This implies that $F_\theta + \chi_\theta$ is zero at these points because B is zero there, which constitutes the conditions for the two circulations.

The boundary conditions are described in detail below.

Eq. (10) is solved by line relaxation, updating lines of constant θ. The annular calculation region is swept back and forth in circumferential direction using a rotated difference operator in supersonic regions to get a locally correct upwind differencing.

The streamline pattern in the calculation plane is illustrated for a typical case in Fig. 3.

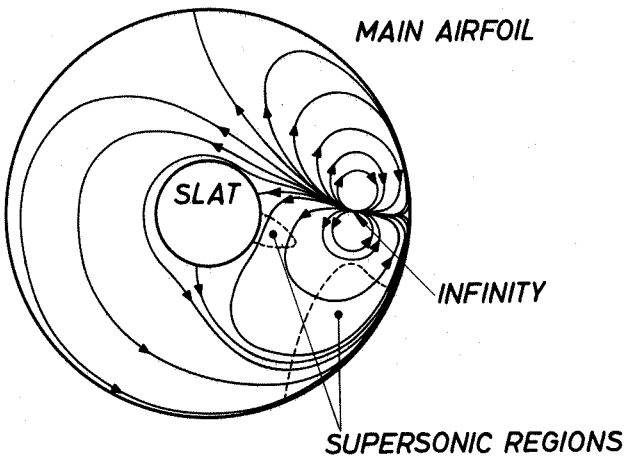

Fig. 3 Streamline pattern in the computational plane

Boundary conditions for analysis and design

When running the program in mixed analysis-design mode the boundary conditions for the potential equation (10) are Neumann conditions for part of the boundaries and Dirichlet conditions for the rest. The Neumann conditions which prescribe zero normal velocity are

$$F_r + \chi_r = 0 \qquad (11)$$

along the corresponding boundary. Numerically this condition is applied by calculating χ in dummy mesh points inside the boundary from

$$\frac{1}{2\Delta r}(\chi_{i,b+1} - \chi_{i,b-1}) = -F_r$$

where i indicates the mesh point in tangential direction and b is the boundary index.

Along a boundary part where design mode is applied the potential values along the boundary are calculated from a prescribed pressure distribution. The potential is obtained using Eq. (7b) which can be written

$$\chi_\theta = q_2 Br - F_\theta \qquad (12)$$

During the relaxation process the boundary value of q_2 used in Eq. (12) is determined from the prescribed pressure coefficient C_p and the normal velocity q_1 which is known for the previous relaxation level. Alternatively q_2 could be related directly to C_p assuming $q_1=0$, because after a few loops including new mappings the contour has almost zero q_1.

When calculating q_2 along the boundary in analysis mode central differences are used for χ_θ. If in design mode a new potential value in the point i, b is calculated in the analogous way from Eq. (12) one obtains

$$\chi_{i,b} = \chi_{i-2,b} + 2\Delta\theta \ (q_2 Br - F_\theta)_{i-1,b} \qquad (13)$$

However, this technique uncouples the odd and even point potentials, noted also by Tranen[8]. To avoid the resulting convergence problems the following formula was used to calculate new potential values

$$\chi_{i,b} = \chi_{i-1,b} + \frac{\Delta\theta}{2}\left[(q_2Br)_{i,b} + (q_2Br)_{i-1,b} - (F_\theta)_{i,b} - (F_\theta)_{i-1,b}\right] \quad (14)$$

For simplicity all the formulas are written without the coordinate stretching included.

The boundary point potentials were updated only when the sweep direction coincided with the local flow direction. Some underrelaxation was used in the updating process for $\chi_{i,b}$, that is, a new value for updating level n+1 was obtained using

$$\chi^{n+1}_{i,b} = \chi^{n}_{i,b} + \omega(\tilde{\chi}^{n+1}_{i,b} - \chi^{n}_{i,b}) \quad (15)$$

where $\tilde{\chi}^{n+1}_{i,b}$ is the potential obtained from Eq. (14).

The potential values in the dummy points inside the boundary were obtained after the corresponding lines had been updated. They were calculated by applying the potential equation to the boundary points.

After the relaxation process had converged a new contour was integrated based on the calculated normal and tangential velocity distribution along the boundary. If the inverse mode part of the boundary ended before a trailing edge the contour integration was yet continued to the trailing edge.

When integrating a new boundary the components in the physical x- and y-direction (u,v) of the boundary velocity vector were first determined. To get high accuracy it is essential that only the change in the contour is determined by the integration process. Thus the slope changes were integrated using the relation

$$\Delta y^{n+1} = \int_{x_0}^{x}\left[\left(\frac{v}{u}\right)^{n+1} - \left(\frac{v}{u}\right)^{n}\right]dx \quad (16)$$

where x_0 is the starting point of the inverse boundary conditions. $(v/u)^{n+1}$ is the new velocity quotient and $(v/u)^n$ is the previous one, that is the slope dy/dx of the present contour.

The integration from one point to the next was performed using local polynomial fitting through integrand points.

Because the calculations to get a new contour are based on the metric for the previous contour an inverse mode run (i.e. a mixed analysis-design mode run) should be followed by a new mapping and an analysis mode run. For cases where the prescribed pressure distributions differ moderately from those obtained in the original analysis calculation, the design process has often converged sufficiently after 1 or 2 new contour integrations. For cases with large prescribed changes in the pressure distribution more loops might be required, sometimes because the first new shapes might be physically unrealistic and the prescribed pressure has to be changed.

Acceleration of the iterative process

At the infinity point the operator D in Eq. (9) applied to χ normally is singular. This is the main reason for a rather slow convergence rate for the line relaxation process. In Ref. 2 a way of improving the convergence rate was discussed which involved the exclusion of a small region around the infinity point after an initial iteration phase.

Since then a more efficient technique has been applied to speed up the convergence rate. It can be denoted extrapolated relaxation, and has been used by Hafez and Cheng[9], Caughey and Jameson[10] and others. The basic idea is that after a number of relaxation sweeps the error vector is dominated by the eigenvector belonging to its largest eigenvalue. This will be the case if the relaxation matrix has distinct eigenvalues which can be ordered,

$$1 > |\lambda_1| > |\lambda_2| \ldots > |\lambda_N|$$

So, after n+1 iterations, that is when an error eigenvector e_j contributes to the total error vector with a term of the order $\lambda_j^{n+1} \cdot e_j$ the approximate relation

$$e^{(n+1)} \sim \lambda_1 e^{(n)} \quad (17)$$

holds for the error vector defined by

$$e^{(n)} = \chi^{(n)} - \chi \quad (18)$$

where χ is the exact solution of the difference equations. Combining Eqs. (17) and (18) yields an estimate for χ,

$$\chi \sim \chi^{(n+1)} + \frac{\lambda_1}{1-\lambda_1} C^{(n+1)} \quad (19)$$

where $C^{(n+1)}$ is the last potential correction

$$C^{(n+1)} = \chi^{(n+1)} - \chi^{(n)} \quad (20)$$

Because λ_1 normally is close to 1, the extrapolation step in Eq. (19) is the same as a large overcorrection of the potential. In practice the factor $\lambda_1/(1-\lambda_1)$ is usually multiplied by a slightly reducing factor, say 0.8.

The relation (17) also implies the same relations for residuals and corrections,

$$R^{(n+1)} \sim \lambda_1 R^{(n)}, \qquad C^{(n+1)} \sim \lambda_1 C^{(n)} \quad (21)$$

where $R^{(n)}$ is obtained from the difference form of Eq. (10), i.e. $R^{(n)} = D^{(n)}\chi^{(n)} + D^{(n)}F^{(n)} + G^{(n)}$ where $D^{(n)}$ is the difference operator corresponding to D.

In order to determine when the accelerations can be made during the iterative process the residual quotients $R^{(n+1)}/R^{(n)}$ where computed for a certain number of the mesh points after each iteration. When

the values of this quotient in the studied points were sufficiently close together according to some statistical measure the extrapolation was made.

Applying the acceleration technique yields a considerable improvement of the overall convergence rate, as illustrated in Fig. 4.

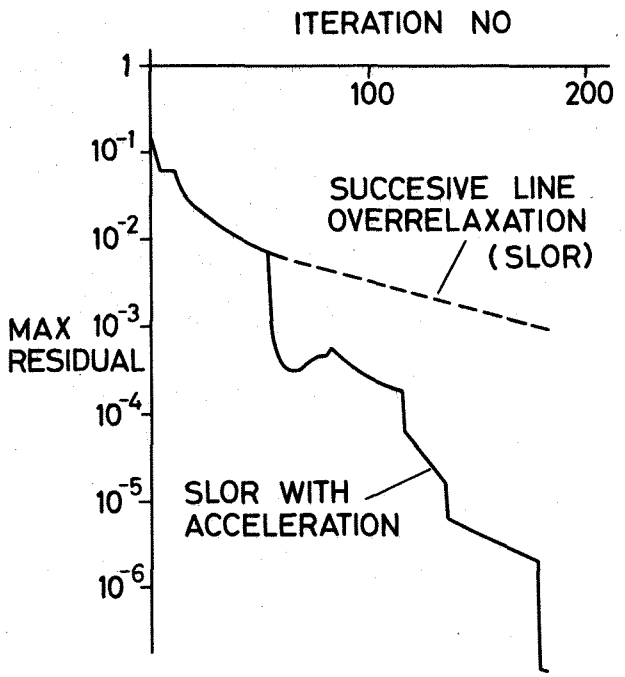

Fig. 4 Time history for iterative processes

Viscus corrections

A comparison between results of the present inviscid method and experiments shows in many cases strong viscous effects. A first attempt to add laminar and turbulent boundary layers has been made by Grossman and Volpe[3] indicating that aside regular boundary layer effects the influence of laminar separation bubbles as well as turbulent separation is dominant.

Therefore in the present program system the viscous effects were taken into account using procedures known to work for high lift devices in low speed using simplified models for laminar separation bubbles and confluent boundary layers. Due to its availability it was decided to use as a first attempt the viscous models of Goradia et al[11] which use integral methods for the boundary layer calculations. Considering the general uncertainties in the modelling of separated regions, confluent boundary layers, shock-wave boundary layer interactions etc, it does not seem to pay off to use rather costly finite difference procedures for the boundary layer calculations.

The boundary layer methods and viscous models used are (for a detailed description see Ref. 11)

- Laminar boundary layer integral method based on the similar solutions of Cohen and Reshotko.
- Transition correlated by Goradia to the Schlichting-Ulrich instability criterion.
- Laminar separation bubbles and laminar stall due to Goradia's semiempirical correlations based on the following cycle:

  stable or unstable? - if unstable test on transition - if no transition apply the Goradia-Lyman criterion for laminar stall prediction.

  The result will be either a short or long laminar separation bubble with turbulent reattachment or bubble burst with stall. In case of stall the calculation will stop.
- Turbulent boundary layer integral method based on Nash using modified Coles profiles. At present there is no model included for turbulent separation in compressible flow.
- Confluent boundary layers using Goradias model.

To compute the total flow field around a two-element airfoil system the viscous models and the present inviscid method are coupled to a program system which runs iteratively the inviscid and viscous part until a converged solution is obtained. The inviscid part provides the velocity distribution along the surfaces which is used by the viscous part to compute the displacement thickness. This is added to the geometric airfoil shapes to get the equivalent viscous shapes, which are used in a new inviscid calculation etc. To guarantee the stability of this procedure some underrelaxation is applied when calculating the displacement thickness using the relation

$$\delta^{*n+1} = \omega_1 \tilde{\delta}^{*n+1} + (1-\omega_1)\delta^{*n}$$

where $\tilde{\delta}^{*n+1}$ is the result of the latest boundary layer calculation.

The present approach is used instead of the more elegant equivalent source model in Ref. 3 because of the rather large displacement effects which are obtained in separated regions. It is felt that regions of this type are more easily treated in terms of equivalent shapes than normal velocity distributions along the wall.

3. Results and discussion

Design calculations

A series of calculations was made for a NACA 64A010 with slat, taken from Ref. 12. Fig. 5 shows the pressure distribution around the original slat and the inverse mode results when a rather large pressure modification on the slat lower surface was introduced. The prescribed pressure was drawn just by free hand and thus was not expected to give a closed airfoil. The resulting shape was found to have a finite trailing edge thickness as seen from Fig. 6. The pressure was considered sufficiently converged after 3 inverse loops. The convergence rate of the relaxation process in a mixed analysis-design mode run was found to be the same as in pure analysis runs except when the difference between prescribed pressure and analysis pressure is very large, as in the first inverse run in the present

case.

To study the effect of a pressure change on the slat upper surface the modification shown in Fig. 7 was made and one inverse loop was performed. The resulting pressure is seen to come rather close to the prescribed pressure. This case should be considered only as a numerical example, because in a real flow large viscous effects would occur close to the trailing edge.

To see the effect of removing the slat trailing edge thickness, the size of which is not realistic in a real design, the final shape in Fig. 6 was modified by changing the lower surface linearly as indicated in Fig. 8. This is seen to have a significant effect on the lower surface pressure, partly explainable in terms of a smaller "lower surface angle of attack".

It was noticed that in the cases mentioned here the main airfoil pressure distribution was very unsensitive to changes in the slat shape as shown by the example in Fig. 9 for the first lower surface modification (Figs. 5, 6).

The configuration in Fig. 10 is a 12 % thick supercritical airfoil denoted DO-A4 with slat, designed at Dornier. The original slat with a "free hand" modification of the lower surface as shown in the figure was used first to get a pressure distribution not too far off the experimental data which indicate a large separated region on the lower surface. The goal was to find the displacement thickness of that region by using the measured pressure distribution in inverse calculations. No attempt was made to modify the main airfoil shape although the viscous effects on that are large. Therefore a lower angle of attack was used for the whole configuration which gave good agreement with the measured pressure distribution on the slat upper surface as seen in Fig. 10. The lower surface pressure distribution used in the mixed analysis-design calculations is seen in Fig. 11 together with the resulting pressure and shape after 4 inverse loops. The last inverse loop was performed on a refined grid containing 64×44 points.

The pressure is considered sufficiently converged towards the prescribed pressure and the resulting lower surface contour is seen to represent a very large separated region.

Results with viscous corrections

The viscous results for a low speed case shown in Fig. 12 prove the iterative procedure to work correctly. Fig. 13 presents viscous results for basically the same airfoil-slat configuration as was used for the inverse calculations shown in Fig. 11. The differences consist in a slightly modified nose region of the main airfoil and that the viscous calculations of course were based on the true physical shapes. Furthermore the viscous calculations were performed for the angle of attack used in the measurements while a smaller angle of attack was used in the inverse calculations.

While the viscous calculations show quite an improved agreement with the experimental data for the main airfoil the results for the slat still are quite off due to the large separated region on its lower surface. In Fig. 14 is shown the marked difference between the displacement surface calculated with the viscous program part and that obtained in the inverse mode calculations. The viscous calculation technique used here has no model for large separated regions, so the displacement thickness obtained after the program indicated laminar separation of long bubble type is not physically realistic. The shape calculated in inverse mode runs, on the other hand, should be regarded as somewhat uncertain because there were rather few experimental pressure points (Fig. 11) and the assumption of constant pressure along lines of constant x in the separated region might not be a good approximation in a region of this size.

Parametric study of leading edge slat configurations

While there exists a rather broad knowledge on the design philosophy for good subsonic high lift devices, only little is known on the proper design of slats for transonic speed. In order to get some insight in the dependence of the pressure distribution on Mach number and simple geometric variations of the configurations a series of calculations were performed using a mesh containing 30×22 points.

As a start another DO-A4 slat configuration was studied, shown in Fig. 15 together with pressure distributions for a series of Mach numbers. While the load on the slat is increasing with increasing Mach number the load on the nose part of the main airfoil is seen to decrease.

For a completely different configuration, a NACA 64A (1.33)05 with slat, Fig. 16 presents the Mach number dependence. It is noted that the flow in the slot exhibits the same Mach number dependence as for the previous configuration.

As a parenthesis it might be concluded from the very different slat pressure distributions that on the NACA slat lower surface the risk for a large separated region is much smaller than for the DO-A4 slat. This is because the suction peak on the NACA slat lower surface is located further away from the nose and is followed by a rapid acceleration to higher trailing edge velocity than on the DO-A4 slat.

In Figs. 17-20 the effects are shown of a change in angle of attack, of horizontal and vertical shifts of the slat and of different slat angles.

The increase in load on both slat and main airfoil with increase of angle of attack is natural, Fig. 17, but it is interesting to notice that the flow in the slot is almost independent of the angle of attack.

Figs. 18-20 show that the most important slat position parameter is its angle. It can also be concluded that in order to have a relatively high velocity at the slat trailing edge the slot should be only slightly converging in the flow direction. To decrease the tendency towards large separated regions on the slat lower surface, the high trailing edge velocity should be combined with a small nose suction peak. This requires a rather subtle combination of the position parameters, and from the figures it is seen that position 2 in Fig. 18

seems to be the best in this respect. Position 5 in Fig. 20 has an even smaller suction peak but here the slat is too much loaded and the main airfoil nose is completely unloaded.

The odd pressure curves close to the slat trailing edge in a few cases are due to high sensitivity to a slightly inadequate geometric input.

4. Concluding remarks

Designing a high lift system for transonic flow means compromising between structural and aerodynamic demands. In that work the present mixed analysis-design mode program is a very effective tool. It requires usually less than 5 loops (new mappings) until sufficient convergence is reached, and the relaxation procedure within each loop is normally as fast as in pure analysis mode.

An essential goal for the designer is to get high lift at low cost, that is to avoid strong shock waves and to keep the viscous effects around the two elements as small as possible. As seen in the present paper a region requiring much attention from the boundary layer point of view is the slat lower surface which due to geometric requirements often is given a shape producing separated regions.

The viscous calculation capability used in the present method does not model separated regions adequately, but it will be improved in the near future and is then expected to predict laminar separation regions in a more realistic way. The plans are to include

- the laminar boundary layer integral method of Stock[13]
- the transition criterion of Michel[14]
- criteria of laminar separation bubbles and stall due to Horton[15]
- Horton's correlations for boundary layer quantities of laminar separation bubbles
- the turbulent boundary layer integral method of Stock[13], using Coles profiles.

5. References

1. Grossman, B. and Melnik, R. E., "The numerical computation of the transonic flow over two-element airfoil systems", Proc. of the 5th Int. Conf. on Numerical Methods in Fluid Dynamics, Springer-Verlag, 1976.
2. Arlinger, B. G., "Analysis of two-element high lift systems in transonic flow", ICAS Paper 76-13, 1976.
3. Grossman, B. and Volpe, G., "The viscous transonic flow over two-element airfoil systems", AIAA Paper 77-688, 1977.
4. Jameson, A., "Transonic flow calculations for airfoils and bodies of revolution", Grumman Aerospace Corporation, Aerodynamics Report 390-71-1, 1971.
5. Arlinger, B. G., "Calculation of transonic flow around axisymmetric inlets, AIAA J. Vol 13, Dec. 1975.
6. Murman, E. M. and Cole, J. D., "Calculation of plane steady transonic flows", AIAA J., Vol 9, Jan. 1971.
7. Jameson, A., "Iterative solution of transonic flow over airfoils and wings, including flows at Mach 1", Comm. Pure and Appl. Math., Vol 27, pp 283-309, 1974.
8. Tranen, T. L., "A rapid computer aided transonic airfoil design method", AIAA Paper 74-501, 1974.
9. Hafez, M. M. and Cheng, H. K., "Convergence acceleration and shock fitting for transonic aerodynamic computations", AIAA Paper 75-51, 1975.
10. Caughey, D. A. and Jameson, A., "Accelerated iterative calculation of transonic nacelle flowfields", AIAA Paper 76-100, 1976.
11. Stevens, W. A., Goradia, S. H. and Braden, I.A., "Mathematical model for two-dimensional multicomponent airfoils in viscous flow", NASA CR-1843, 1971.
12. Axelson, J. A. and Stevens, G. L., "Investigation of a slat in several different positions on a NACA 64A010 airfoil for a wide range of subsonic Mach numbers", NACA TN 3129, 1954.
13. Stock, H. W., "Integralverfahren zur Berechnung dreidimensionaler, laminarer und turbulenter Grenzschichten," Dornier FB 77/51B, 1977.
14. Michel, R., "Etude de la transition sur les profiles d'aile", ONERA Report 1/1578A, 1951.
15. Horton, H. P., "A semi-empirical theory for the growth and bursting of laminar separation bubbles", ARC-CP No 1073, 1969.

This work was supported by Saab-Scania, Sweden and the German Ministry of Defence under Contract T/R 421 70005/72403.

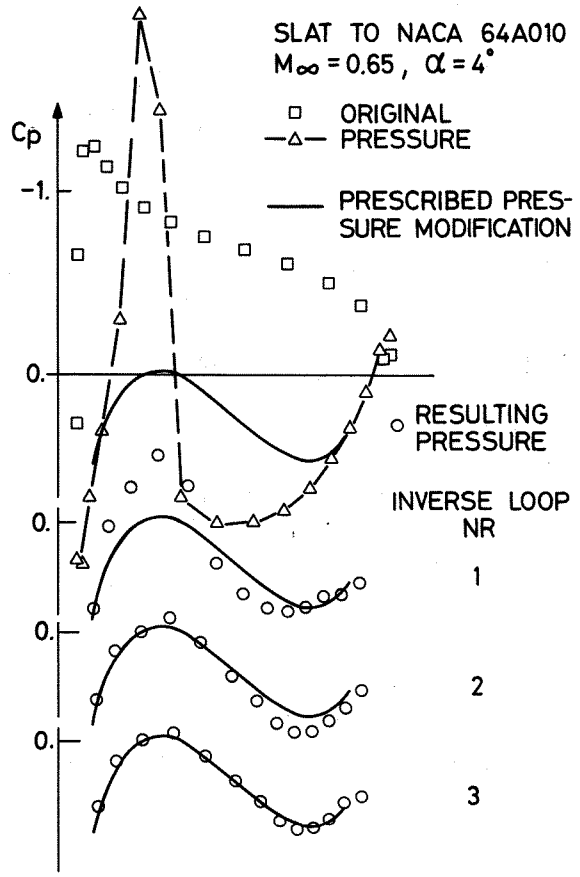

Fig. 5 Redesign process for slat lower surface

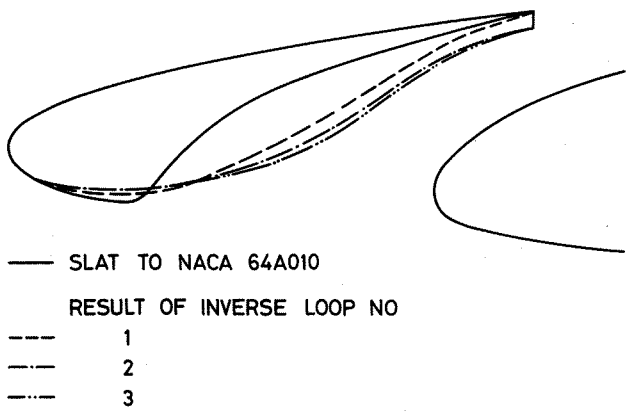

Fig. 6 Successive slat shapes in redesign process

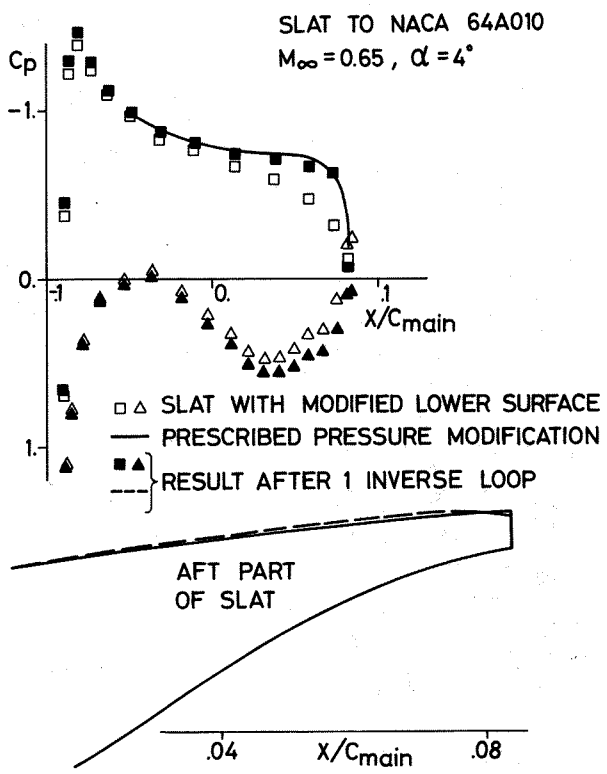

Fig. 7 Modification of slat upper surface

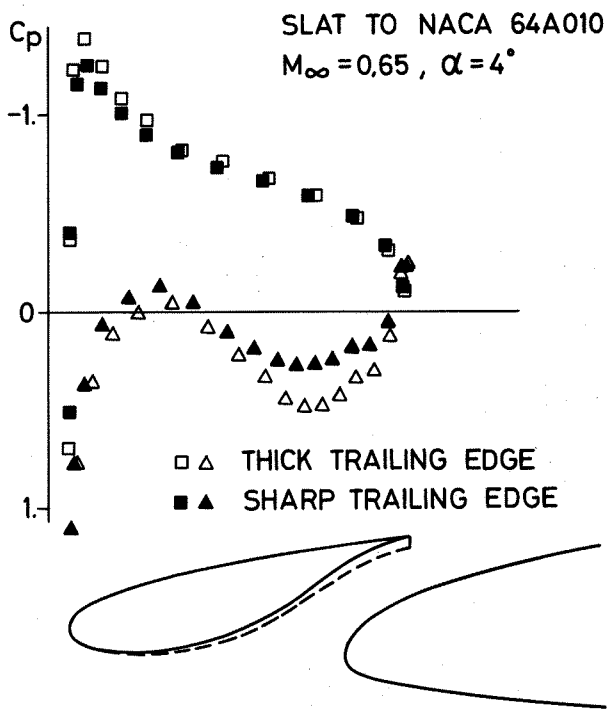

Fig. 8 Effect on slat pressure of removing thick slat trailing edge

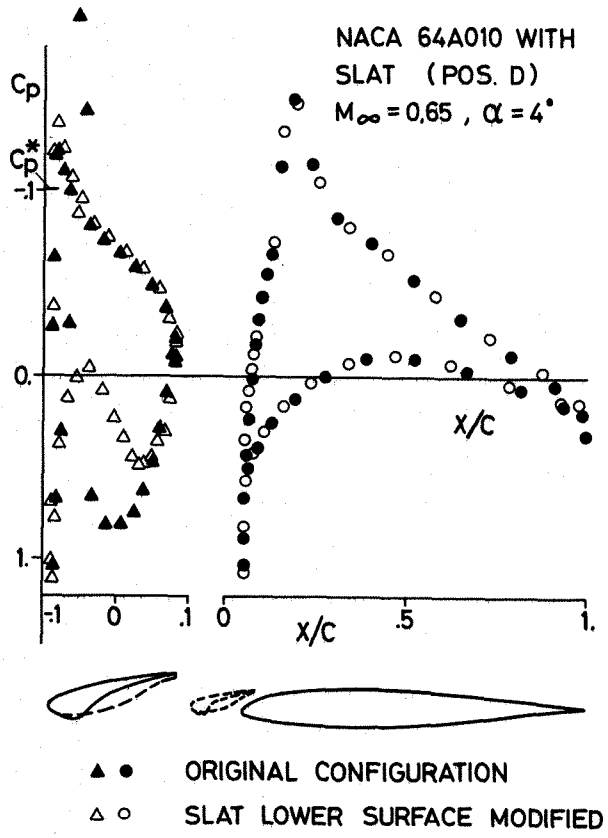

Fig. 9 Effect on main airfoil pressure distribution of modifying the slat

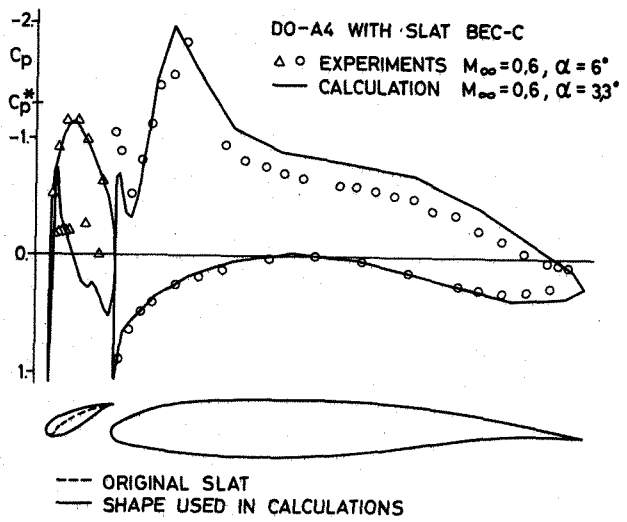

Fig. 10 Analysis of a case with separation on the slat

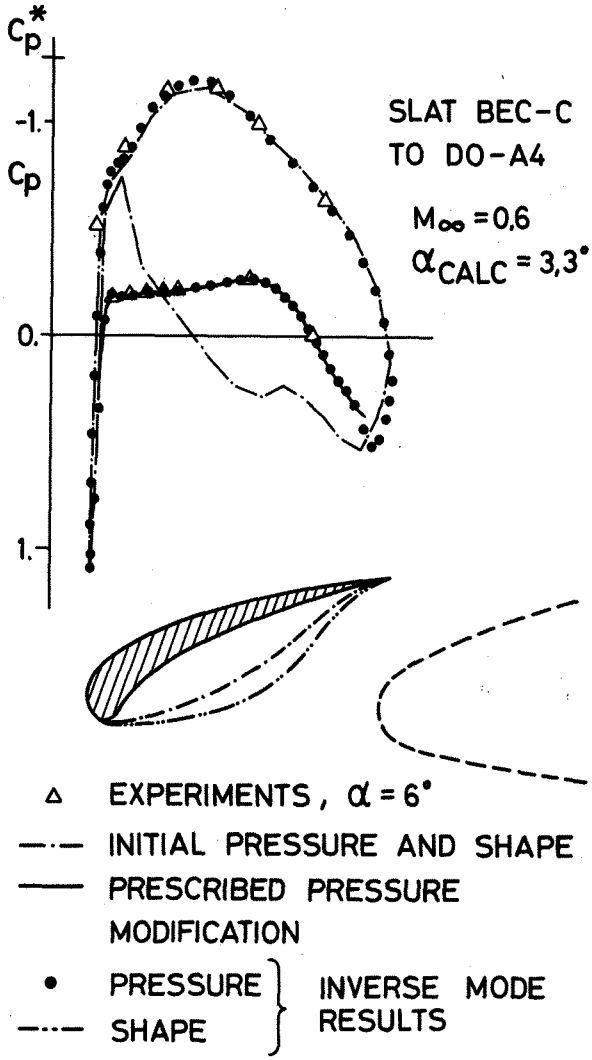

Fig. 11 Slat separation determined by mixed analysis-design mode runs

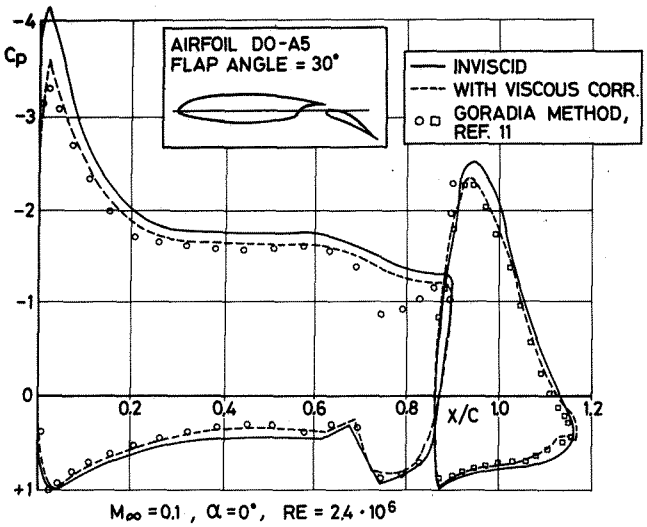

Fig. 12 Effects of viscous corrections in a low speed case

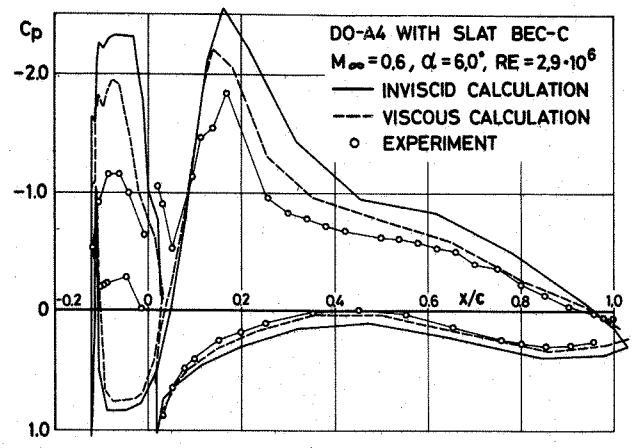

Fig. 13 Results for case with strong viscous effects

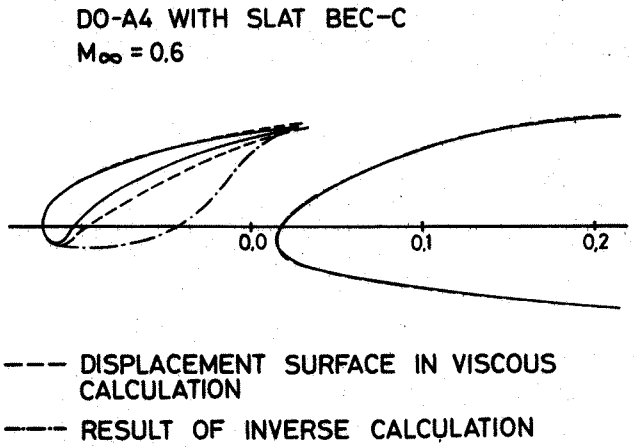

Fig. 14 Slat lower surface shapes

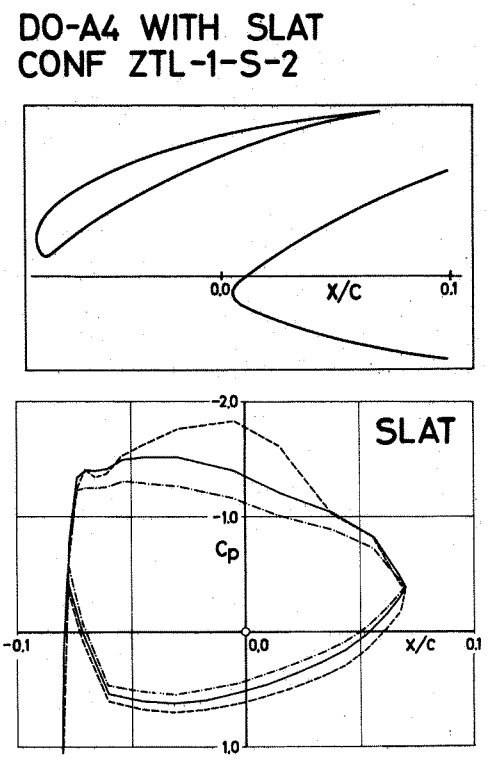

Figure continues

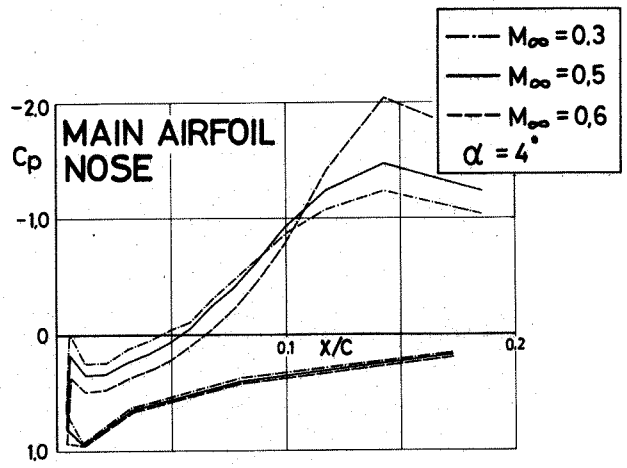

Fig. 15 Effect of Mach number change

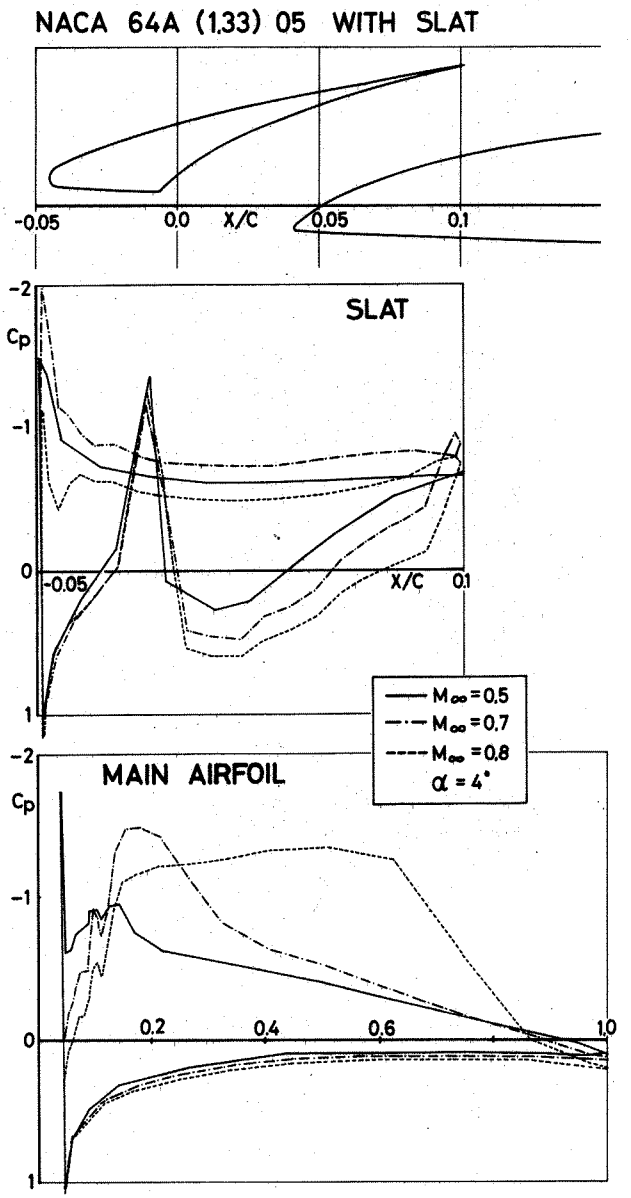

Fig. 16 Effect of Mach number change

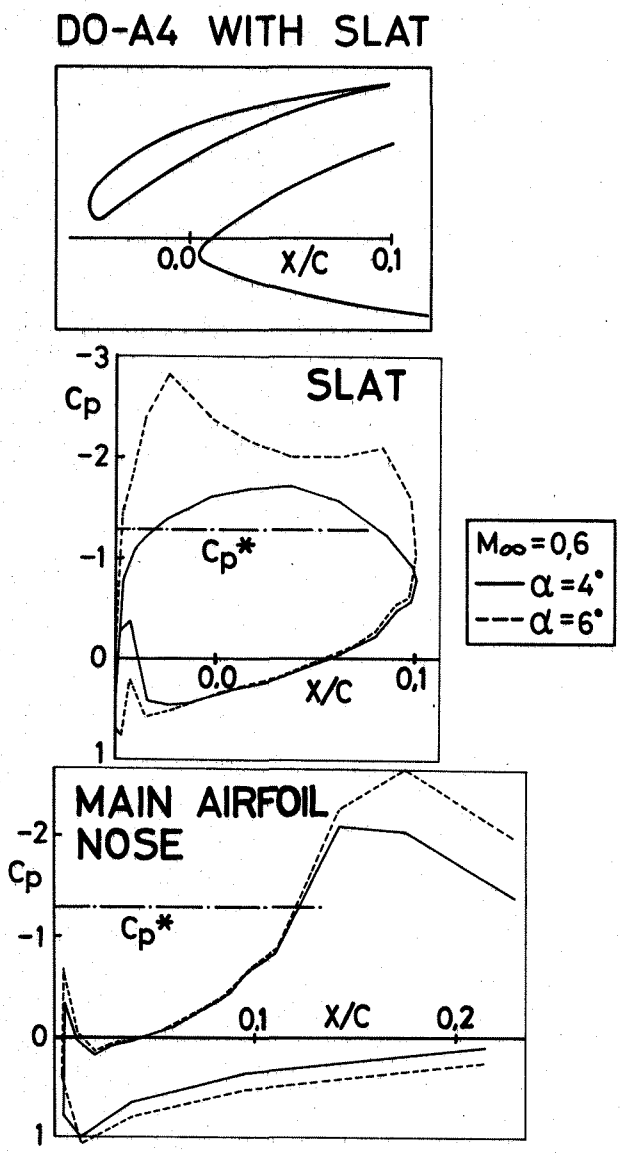

Fig. 17 Effect of change in angle of attack

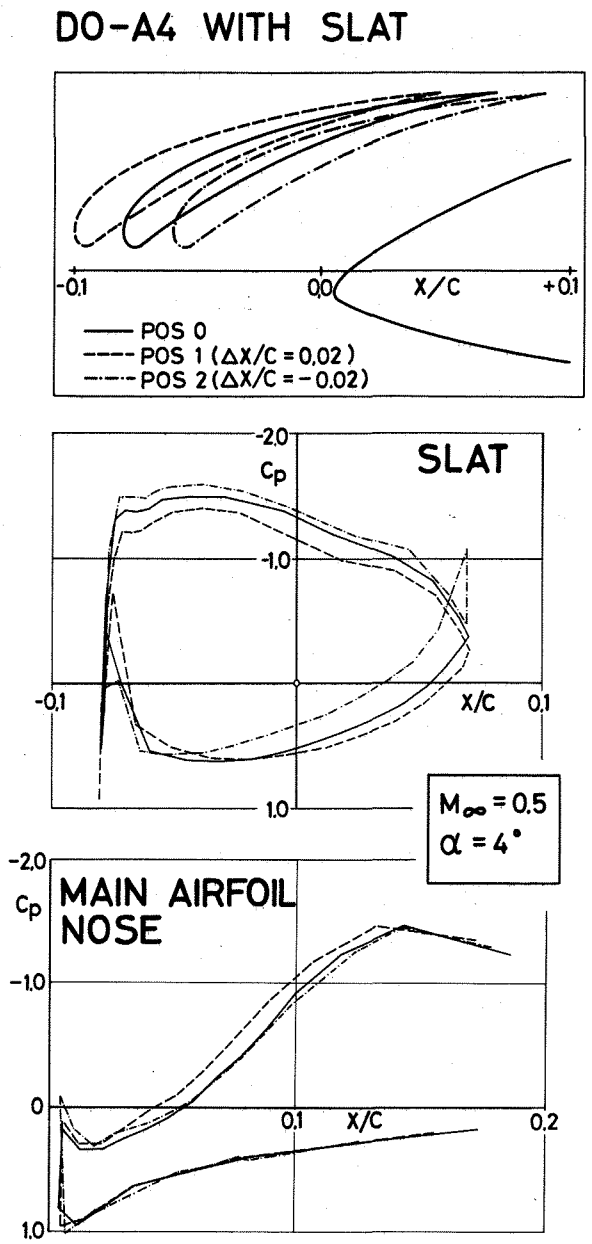

Fig. 18 Effect of horizontal shift of slat position

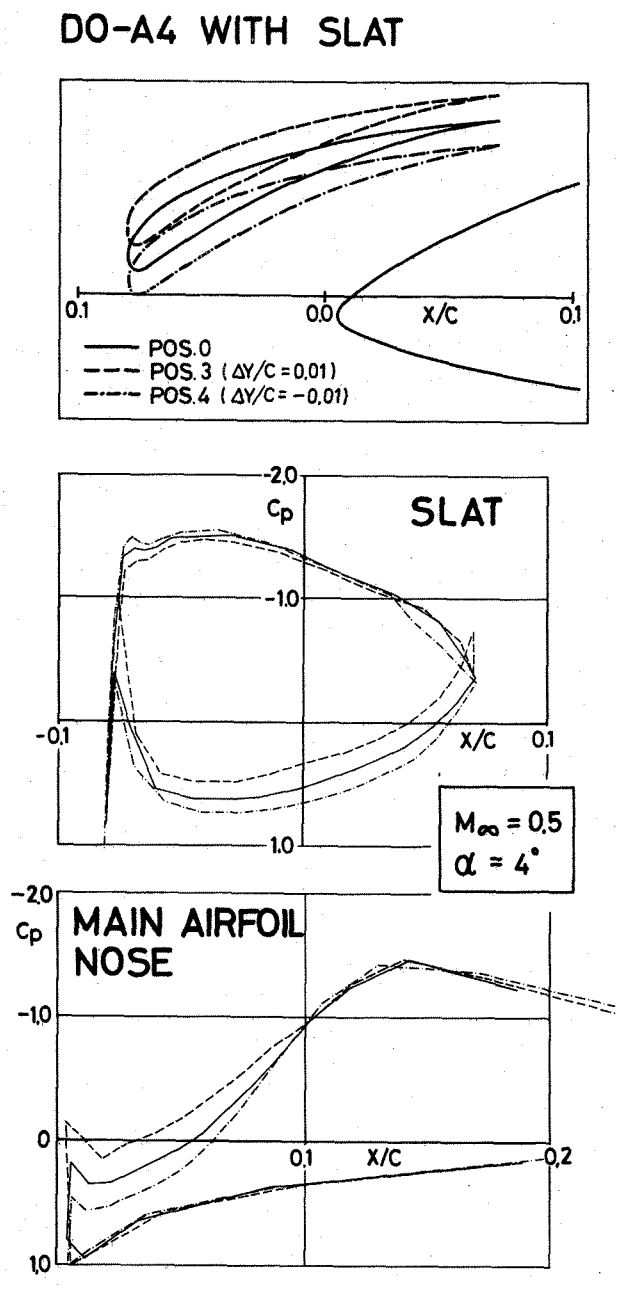

Fig. 19 Effect of vertical shift of slat position

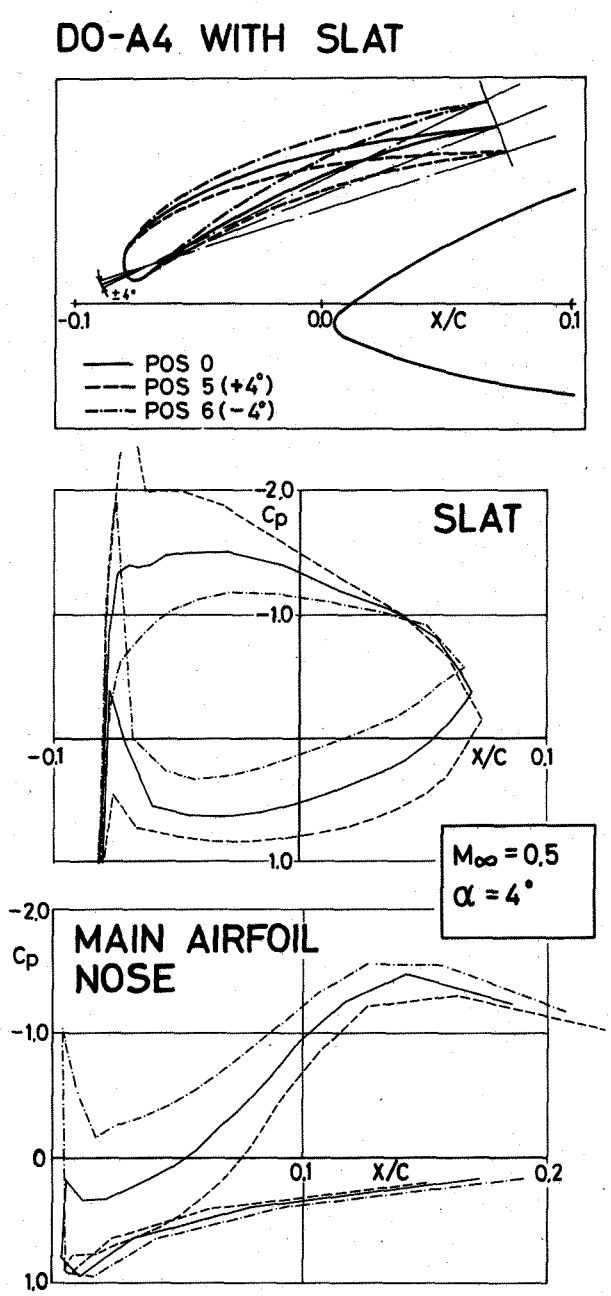

Fig. 20 Effect of change in slat angle